Highlights

Design of Ball-Ramp Dual Clutch Transmission to Reduce Uncertainties in Clutch Actuator and Tie-up Effect

Dong-Hyun Kim, Seibum B. Choi

- A complementary design method of ball-ramp DCT is developed.

- A design constraints for reducing tie-up and improving actuator model is proposed.

- Proposed actuator model and constraints are verfied with powertrain test bench.

Design of Ball-Ramp Dual Clutch Transmission to Reduce Uncertainties in Clutch Actuator and Tie-up Effect

Dong-Hyun Kim[a], Seibum B. Choi[b]

[a]*R&D Division, Hyundai Motor Company, 150 HyundaiYeonguso-ro, Namyang-eup, Hwaseong-si, 18280, Gyeonggi-do, Republic of Korea*
[b]*School of Mechanical, Department of Mechanical Engineering, Korea Advanced Institute of Science and Technologyy (KAIST), 291 Daehak-ro, Yuseong-gu, 34141, Daejeon, Republic of Korea*

Abstract

Dual-clutch transmissions (DCT) have high efficiency, low drop in tractive force during shifting, and fast shifting is possible. However, it is infeasible to measure clutch torque due to cost and durability problems, and difficult to control clutch torque due to change in friction coefficient. Also, the energy consumed by the actuator for maintaining engagement is large. To address these limitations, a Ball-Ramp DCT (BR-DCT) was developed based on the self-energizing principle. The BR-DCT can reduce energy consumption of the clutch actuator. In addition, it is possible to reduce the uncertainties in actuator by using only measurable values to calculate the actuator input; and, when a tie-up occurs in which two clutches are engaged at the same time, the magnitude of negative torque can be reduced. However, design constraints for implementing last two features were not addressed in previous studies. In this paper, we propose the two design constraints to reduce the uncertainties in actuator and reduce the tie-up effect. For verification, a BR-DCT prototype and powertrain test bench were manufactured with the design constraints. As a result of the shift experiment, it was verified that accuracy of the actuator model can be improved, and the tie-up effect can be reduced.

Keywords: Dual-clutch transmission, Ball-ramp mechanism, Self-energizing principle, Mechanical design constraints, Clutch actuator model, Clutch tie-up reduction

1. Introduction

In automobiles, the transmission transmits the power generated from a power source (engine or motor). At this time, the transmission controls the transmitted torque to change the wheel speed or torque. In addition, the use of a transmission maintains an efficient operating point of the power source. And the magnitude and direction of the torque transmitted to the wheel change according to the result of the shift control. Therefore, the efficiency and control performance of the transmission directly affects the energy efficiency, acceleration performance, and ride comfort of the vehicle [1, 2]. As a result, research on transmission has been focused on improving transmission efficiency and control performance.

Among various transmission types, Manual Transmission (MT) is the most basic transmission in which the driver performs shift control. This transmission uses a clutch that can generate friction torque to transmit the power generated from the power source. Therefore, MT has good transmission efficiency, but riding comfort or acceleration performance may decrease depending on the control result of clutch torque [3, 4]. Since the driver performs shift control, the riding comfort or acceleration performance may change according to the driver's ability to shift. For this reason, fatigue increases and vehicle performance varies depending on the driver.

To solve this problem, Automated Manual Transmission (AMT) was developed [5]. AMT is a transmission that automates the MT shifting process through an actuator. AMT uses a gear selector to select the gear to be shifted and performs clutch control with a clutch actuator. Therefore, it is possible to reduce driver fatigue and keep the vehicle performance constant. However, it still takes a long time to shift. In addition, it is infeasible to install a sensor that can measure the torque of a clutch or a drive shaft in a typical vehicle due to cost, durability, and size issues. For this reason, the clutch torque cannot be measured when performing clutch torque control, and control performance is reduced. In addition, since the clutch needs to be disengaged during shifting, a torque interruption in which the transmitted torque becomes zero occurs [6]. To address these shortcomings, Automated Transmission (AT) using a torque converter was developed. AT consists of several planetary gear sets and performs shifting by crossing clutches or brakes. In addition, by crossing the transmission torque of the clutch, it is possible to shift faster than AMT or MT and eliminate torque interruption. Also, the clutch system of the MT and AMT was replaced with a torque converter
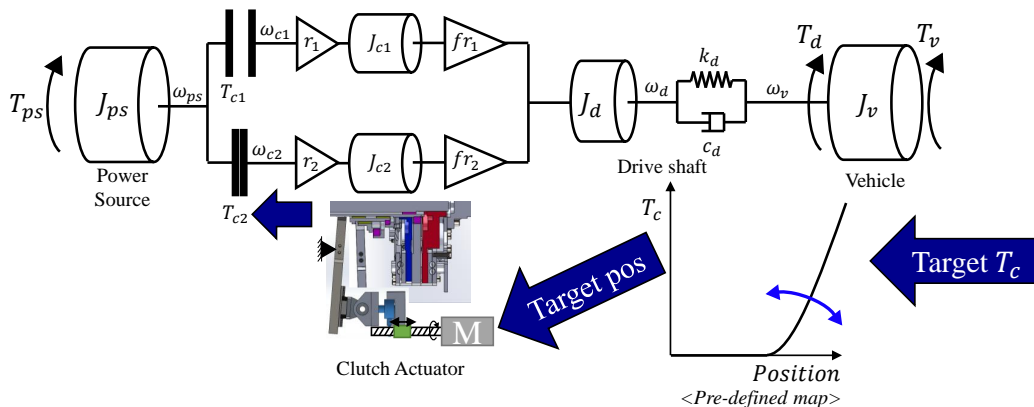
Figure 1: Clutch torque control method using pre-defined actuator map of conventional DCT.

to improve the launch performance at low speed by using the amplification effect. Since the torque converter transmits the power by a fluid, the AT can absorb most of the shift shocks caused by the absence of clutch torque measurement[7]. Therefore, the AT has low shift shock even when shifting control is performed with the clutch actuator model in which uncertainty is not considered. However, the torque converter used in AT greatly reduces vehicle energy efficiency because of low power transmission efficiency. In addition, power loss resulting from the inevitable slip of the torque converter may deteriorate the acceleration performance of the vehicle[8, 9].

The Dual Clutch Transmission (DCT) was developed to compensate for these shortcomings of AT. The DCTs are increased the number of clutches of AMT to two and designed to select even and odd gears for each clutch shaft [10, 11]. The DCT allows fast-shifting by crossing clutches, as in AT, and torque converters are replaced with dual clutches to increase transmission efficiency and decrease transmission power loss[7]. That is, it is possible to increase the energy efficiency and acceleration performance of the vehicle[12, 13]. However, the energy consumption of the actuator to maintain the engagement of the clutch after shifting is large enough to correspond to about 15% of the alternator's power generation. [14] Also, since the clutch torque sensor is usually not installed, the performance of clutch torque control cannot be guaranteed. Therefore, since it is infeasible to measure the clutch torque, the actuator model using the equation of the clutch friction torque is used [15, 16, 17, 18]. In general, an inverse model of the actu-

3

ator is used to generate the target position of the clutch actuator used as an input. (Fig. 1) At this time, since the equation of the clutch friction torque is used, the friction coefficient of the clutch is used as a parameter. Here, model uncertainty occurs due to the change in the friction coefficient. This model uncertainty made it difficult to calculate the accurate actuator input for generating the clutch torque, and thus the control performance was deteriorated[19, 20, 21, 14]. Additionally, if both clutch shafts (connected to the final gear) are engaged with the power source, the clutch shaft may be damaged due to a tie-up phenomenon in which a large torque is applied to each clutch shaft[22].

Some studies have been conducted to address these shortcomings of DCT. First, dry-type rack-pinion DCT (RP-DCT) with a self-energizing mechanism applied to reduce actuator energy consumption was studied[23, 24, 25]. Additional engagement force can be obtained by utilizing the clutch torque as mechanical feedback of the actuator. In this way, the required power of the clutch actuator to generate the clutch torque is reduced by the self-energizing gain. However, the rack-pinion gear used to implement the self-energizing mechanism reduced controllability by causing friction and backlash. In addition, the size of the clutch pack was required to be largely due to the minimum tooth size of the gear. To solve this problem, dry-type ball-ramp DCT (BR-DCT) was studied[14]. Because the self-energizing principle using the ball-ramp mechanism is applied to the BR-DCT, backlash and friction are eliminated, and it can be implemented with a small size. In a previous study, to secure clutch torque control performance while reducing actuator energy consumption, design constraints that prevent self-locking and maintain engagement even when negative clutch torque occurs were proposed.

Second, various techniques such as adaptation, unknown input observer, and disturbance observer were used to estimate the change in friction coefficient of DCT, which is the uncertainty that occurs in the clutch actuator[26, 27, 28]. However, it was not possible to accurately estimate the friction coefficient, which changes rapidly due to various factors such as slip speed, torque, and temperature of the clutch. However, if the modeling equations of the self-energizing clutch actuator of BR-DCT proposed in previous studies are used, uncertainty can be reduced. However, in previous studies, there was not enough discussion on the establishment of modeling of the actuator using self-energizing, and the reduction of the uncertainties in the clutch actuator was not clearly presented.

Third, studies to reduce tie-up were also conducted. Tie-up is a phe-
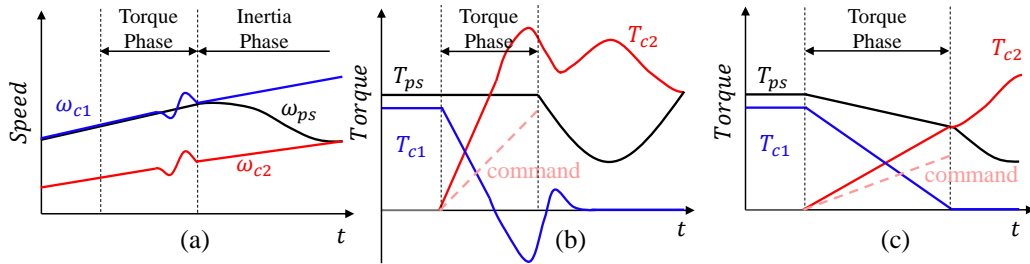
Figure 2: Example of tie-up occurring during shift control. (a) Speed, (b) Torque, (c) Example of conservative torque phase control to reduce tie-up effect.

nomenon in which negative torque is generated from the off-going clutch, and torque is transmitted to both clutches. In (b) of the Fig. 2, the tie-up is graphically expressed. If the off-going clutch does not disengage even when the torque becomes 0, negative torque is generated. At this time, a large torque is applied to the on-coming clutch shaft, which may cause shaft damage. In (a) of the Fig. 2, the shift control of the DCT is divided into the Torque Phase (TP), which exchanges torque between the on-coming clutch and the off-going clutch, and the Inertia Phase (IP), which synchronizes the speed between the on-coming clutch and the power source. As shown in (c) of the 2, the normally mass-produced DCT shift controller delays the torque rise of the on-coming clutch by increasing the shift time to prevent tie-up or reducing the torque of the power source to prevent flare. However, this method increases the time of the TP or reduces the transmission torque, so that the shifting performance has deteriorated. To solve the disadvantages of the conventional method, a control method using iterative control has been proposed[29]. In this study, the characteristic of iterative control in which control parameters change based on repeated shift data was applied. At this time, this study tried to reduce the tie-up phenomenon by changing two parameters. (Maximum filling pressure and filling time) However, since time is still used as a parameter, performance degradation may occur due to an increase in shift time. Specifically, this method does not pose a problem because it is performed before shifting in a general shift situation. However, when the driver power demand increases rapidly, such as power on down shift, filling starts at the same time as the shift starts. Accordingly, an increase in the filling time may increase the shift time in a situation such as power on down shift, thereby degrading shift performance. Tie-up is a problem that occurs due to the characteristics of hardware, but this study has limitations

in performance because it solves the shortcomings of hardware with software.

To solve the shortcomings of the previous studies, this paper proposes the design constraints for the reducing the uncertainties in the actuator model and reducing the effect of tie-up as follows.

First, the reduction of the uncertainties in the clutch actuator using the self-energizing mechanism is established with the following principle. The self-energizing mechanism allows the clutch torque to interact with the actuator. That is, clutch torque can be expressed using only measurable values without friction coefficient. This method is different from the clutch actuator model used in the conventional DCT. In other words, in order to use the friction torque equation of the clutch, the clutch torque is calculated by multiplying the clutch disk compression (obtained by the actuator encoder) by the clutch disk friction coefficient[18, 17]. Especially, friction coefficient cannot be obtained with the measurements of the conventional dry type DCT, the friction coefficient had to be assumed as a constant. Based on this problem, a study on the clutch torque observer, which is a method to estimate by applying adaptive logic to the friction coefficient, was also conducted[18, 17]. However, model uncertainty can be greatly reduced because BR-DCT can remove the friction coefficient from the actuator model by using a self-energizing mechanism. Therefore, if BR-DCT is used, input calculation using an accurate clutch actuator model is possible. Accordingly, the uncertainty of the actuator model is also significantly reduced.

Second, the method of reducing the tie-up effect by using the self-energizing principle is performed by the following principle. According to previous research, the magnitude of self-energizing gain varies according to the direction of clutch torque[14]. At this time, the magnitude of the self-energizing gain in the reverse direction is always smaller than that in the forward direction. If the magnitude of the self-energizing inverse gain is less than 1, engagement cannot be maintained. Therefore, there is a need for a constraint that can maintain the engagement when the reverse clutch torque occurs. Paradoxically, using this feature can reduce the tie-up effect. By adjusting the self-energizing gain, the maximum transmitted friction torques of the forward and reverse torques can be adjusted. If the maximum transmittable torque in the reverse direction is reduced, the clutch disengages even with a small reverse torque and slip occurs. In other words, because the dynamic friction torque smaller than the static friction torque is generated, the negative torque is reduced and the tie-up effect is alleviated. Therefore, it is necessary to propose design constraints to reduce the tie-up effect.

6

In this paper, design constraints that complement the shortcomings of BR-DCT proposed in previous studies are proposed. Therefore, the contribution of the paper can be organized as follows. First, we propose a new clutch actuator model that can remove the clutch friction coefficient. Second, we propose the design constraints of BR-DCT to reduce the uncertainties in the actuator model. Third, we propose the design constraints of BR-DCT that can reduce the tie-up effect. The clutch actuator model and design constraints proposed in this paper are verified on a powertrain test bench equipped with BR-DCT.

The structure of this paper is as follows. In Section 2, equations for establishing an improved clutch actuator model to reduce the uncertainties and design constraints for using them are presented. In addition, we propose design constraints to reduce the tie-up effect. To verify the proposed method, Section 3 experiments to verify the improved clutch actuator model and the tie-up phenomenon reduction effect with a test bench designed with a closed-loop shift controller. Finally, this work is concluded in Section 4.

2. Design Constraints for Ball-ramp DCT

The target system of this paper, BR-DCT, can be expressed as a free body diagram as shown in Fig. 3. From this figure, the operating principle of BR-DCT can be briefly reviewed. First, F_r is applied from the clutch actuator. This force rotates the magenta lever based on the hinge point of the pressure plate. Here, since the vehicle side plate becomes a supporting point, a vertical force F_a and a rotational force F_t are applied to the pressure plate. These forces generate rotation-translational motion of the pressure plate. Here, on the pressure plate, the force F_s of the return spring acts as a returning force, and the red and brown ball-ramp mechanism acts as a constraint of movement. Therefore, the pressure plate receives torque in the direction inclined by the ramp angle α. When the clutch friction torque T_c is applied to the pressure plate, torque is obtained. This torque is converted to a normal force N that compresses the clutch disk due to the ball-ramp mechanism. Through this process, engagement of the clutch occurs. Disengagement is the reverse of the above process.

The force and torque balance equation that can be derived from the figure is as follows [14].

$$J_p \ddot{\theta}_p = F_t R_a + T_c - F_b R_b \sin \alpha - F_s R_s \sin \beta \tag{1}$$

Table 1: Description of each notations

Symbol	Name	Symbol	Name
N	Clutch disk normal force	μ	Clutch disk friction coefficient
a	Release bearing force moment arm	b	Lever reaction force moment arm
a_f	Release bearing friction force moment arm	b_f	Lever reaction friction force moment arm
$L(\theta_{BR})$	Translation to rotation conversion ratio	α	Ramp angle
β	Return spring angle	F_r	Release bearing force
F_a	Clutch actuator force	F_t	Clutch actuator rotational force
F_s	Return spring force	F_b	Ball reaction force
R_a	Lever actuation radius	R_b	Ball actuation radius
R_c	Clutch disk effective radius	R_s	Return spring actuation radius
T_c	Clutch friction torque	T_{ps}	Power source torque
θ_p	Pressure plate rotation angle	θ_c	Vehicle side plate rotation angle
θ_{BR}	Ball-ramp actuation angle	x_p	Pressure plate displacement
J_p	Pressure plate inertia	J_c	Vehicle side plate inertia
m_p	Pressure plate mass	m_c	Vehicle side plate mass
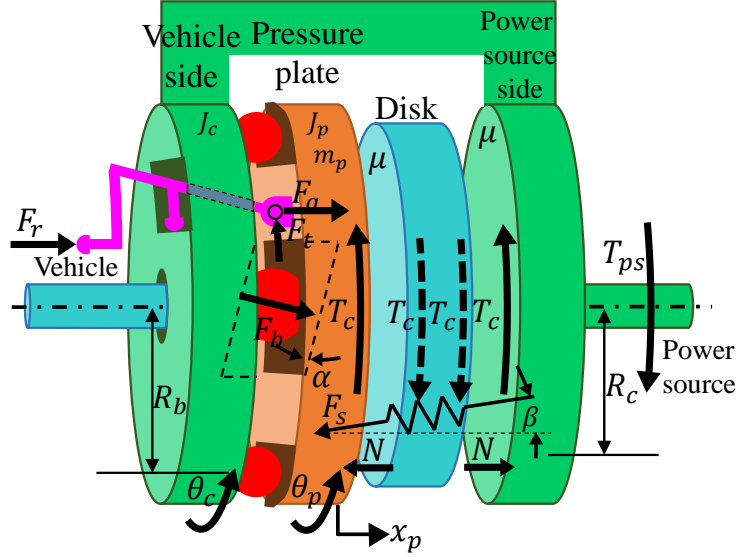
Figure 3: Free body diagram of the BR-DCT.

$$F_t = L(\theta_{BR})F_a \tag{2}$$

$$m_p \ddot{x}_p = F_a + F_b \cos\alpha - F_s \cos\beta - N \tag{3}$$

$$T_c = \mu N R_c \tag{4}$$

$$x_p = R_b \theta_{BR} \tan\alpha \tag{5}$$

$$\theta_{BR} = \theta_p - \theta_c \tag{6}$$

(1), (2) and (3) are the torque, lever and force balance equations, and (4), (5) and (6) are the clutch friction torque equation and ball-ramp mechanism constraints, respectively. Here, $L(\theta_{BR})$ is expressed as follows using the free body diagram (Fig. 4) of the actuation lever.

$$\frac{\mu_L^2 a_f + \mu_L b - \mu_L b_f + a}{\mu_L^2 b_f + \mu_L a_f - \mu_L a + b} F_a = L(\theta_{BR})F_a = F_t \tag{7}$$

where, a, b, a_f and b_f are moment arms of F_r, N_L, N_{Lf} and F_{rf}, respectively, and change according to θ_{BR}. μ_L is the coefficient of friction between the lever and the pressure plate.
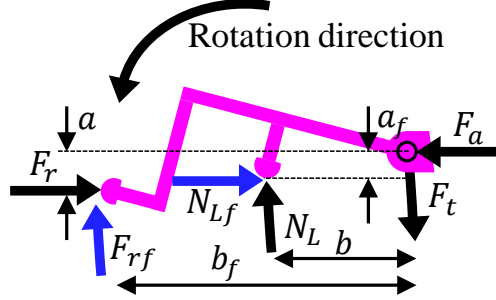
Figure 4: Free body diagram of self-energizing actuation lever. F_r is the force exerted by the release bearing on the clutch actuator lever, and N_L is the rotational reaction force generated from the vehicle side plate. In addition, F_{rf} and N_{Lf} are frictional forces generated by F_L and N_L, respectively.

Using the above equations, the clutch torque equation can be derived as follows. In this case, the inertia term of the pressure plate is very small and is therefore ignored.

$$T_c = \mu R_c \frac{R_b \tan \alpha + L(\theta_{BR}) R_a}{R_b \tan \alpha - \mu R_c} F_a - \mu R_c \frac{R_s \sin \beta + R_b \tan \alpha \cos \beta}{R_b \tan \alpha - \mu R_c} F_s \quad (8)$$

$$G = \frac{R_b \tan \alpha + L(\theta_{BR}) R_a}{R_b \tan \alpha - \mu R_c}, G_s = \frac{R_s \sin \beta + R_b \tan \alpha \cos \beta}{R_b \tan \alpha - \mu R_c} \quad (9)$$

In (8), the coefficient of $\mu R_c F_a$ is defined as self-energizing gain (G), and the coefficient of $\mu R_c F_s$ is defined as return spring gain (G_s).

2.1. Basic Design Constraints

Conventional DCT can be expressed as $F_r = F_a$ because the actuation lever does not rotate. Also, since there is no self-energizing mechanism, it is defined as $G = 1$ and $G_s = 1$. Therefore, clutch friction torque equation (8) can modified as follows.

$$T_c = \mu R_c F_a - \mu R_c F_s \quad (10)$$

However, in BR-DCT, G and G_s are determined according to the design parameters. Therefore, if the parameter is designed so that G is greater

than 1 and G_s is close to 0, the energy consumption of the actuator of the BR-DCT can be reduced. At this time, G_s is dependent on the change in β. Referring to the similarity of the values of R_s and R_b, it can be seen that $\sin \beta$ is the dominant element of G_s. Thus, since G_s is proportional to β, β can be minimized to minimize G_s [14].

If the design parameter is selected so that G is smaller than 0, negative F_a is needed to generate T_c. In other words, since T_c occurs without F_a, a self-locking phenomenon that results in a loss of controllability of the clutch torque occurs. Therefore, G must be greater than zero [14].

In the same situation as during power source brake, T_c has a negative value. In this case, (1) and (8) are modified as follows.

$$J\ddot{\theta}_{BR} = F_t R_a - T_c - F_b R_b \sin \alpha - F_s R_s \sin \beta \tag{11}$$

$$T_c = \mu R_c \frac{R_b \tan \alpha + L(\theta_{BR}) R_a}{R_b \tan \alpha + \mu R_c} F_a - \mu R_c \frac{R_s \sin \beta + R_b \tan \alpha \cos \beta}{R_b \tan \alpha + \mu R_c} F_s \tag{12}$$

In (12), the coefficient of $\mu R_c F_a$ is defined as the self-energizing inverse gain (G_{inv}), and the coefficient of $\mu R_c F_s$ is defined as the return spring inverse gain ($G_{s,inv}$). To prevent self-locking even when negative T_c occurs, G_{inv} and $G_{s,inv}$ must be greater than 0. Also, the denominators of G and G_{inv} consist of positive parameters. Thus, the denominator of G_{inv} is always larger than the denominator of G, G_{inv} is always smaller than G. For this reason, a condition is required to maintain engagement when negative T_c occurs. Here, it is assumed that $G_{s,inv} \rightarrow 0$ is based on the actuator energy consumption reduction constraint. In addition, it is assumed that parameters related to the size (R_a, R_b, R_c and $L(\theta_{BR})$) are determined in advance according to the target size. The maximum value of T_c can be expressed by multiplying the maximum torque of the power source by η. ($T_{c,inv,max} = \eta T_{ps,max}$) Here, η represents the ratio of the torque of the maximum inverse clutch torque to the torque of the maximum power source. Thus, $T_{ps,max}$ can be expressed as G and $F_{a,max}$. ($T_{ps,max} = \mu R_c G F_{a,max}$) Therefore, the following constraints can be derived.

$$\eta T_{ps,max} = \eta \mu R_c G F_{a,max} < \mu R_c G_{inv} F_{a,max} \tag{13}$$

When the above constraints are summarized, the design constraints of the BR-DCT proposed in the previous study are as follows.
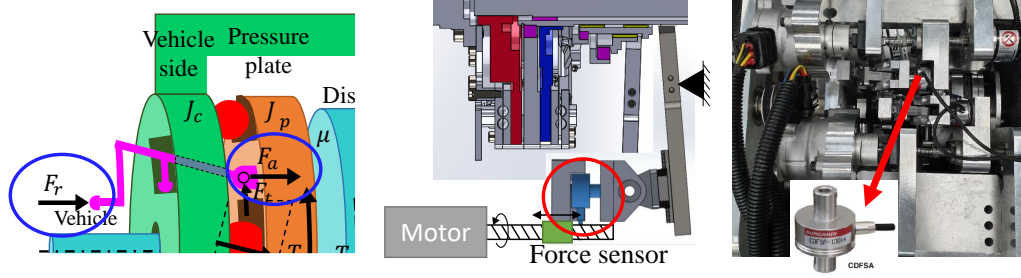
Figure 5: A force sensor was installed to measure F_a. Since the sensor cannot be attached inside the clutch pack, the sensor is installed at the output of the clutch actuator.

1. $\tan \alpha > \mu \frac{R_c}{R_b}$: To avoid self-locking.
2. $G, G_{inv} > 1, \beta > 0, \beta \rightarrow 0(G_s, G_{s,inv} \rightarrow 0)$: To reduce energy consumption of the clutch actuator.
3. $\tan \alpha < \mu \frac{R_c(1+\eta)}{R_b(1+\eta)}$: To hold clutch engaged when negative clutch torque applied.

2.2. Proposed Design Constraints

2.2.1. Eliminate μ from the clutch actuator model

Substituting (4) into the equation (8) and arranging for μ is as follows.

$$\mu = \frac{R_b \tan \alpha}{R_c} - \frac{(R_s \sin \beta + R_b \cos \beta \tan \alpha)F_s}{R_c N} - \frac{(R_b \tan \alpha + L(\theta_{BR})R_a)F_a}{R_c N} \tag{14}$$

Multiplying both sides of equation (14) by $R_c N$ is as follows.

$$T_c = -F_a\{L(\theta_{BR})R_a + R_b \tan \alpha\} + F_s(\sin \beta R_s + \cos \beta R_b \tan \alpha) + R_b \tan \alpha N \tag{15}$$

In (15), $L(\theta_{BR}), \beta, F_s$ and N are variables determined by θ_{BR}. Therefore, using the equation (15), the clutch torque can be expressed by measuring only the position (θ_{BR}) and force (F_a) of the clutch actuator.

However, the actuator force (F_a) needs to be measured by using the current of the actuator motor or by adding a force sensor. In general, a dry-type DCT clutch actuator uses a linear actuator using a ball screw. Due to the friction of the ball screw, force measurement using the current of the actuator motor is less accurate. Therefore, a force sensor can be mounted on the

12

linear actuator output to measure the actuator force (F_a) of the BR-DCT. Actually, this force sensor can measure F_r, as shown in Fig. 5, it can be converted as F_a by using the actuation lever model. Since the maximum force of the actuator is reduced due to the self-energizing effect of the BR-DCT, the capacity or size of the force sensor is small. Therefore, it is relatively easy and inexpensive to mount the sensor on the actuator output.

2.2.2. Reduction of Tie-up Effect

In DCT, the clutch tie-up is caused by a change in the friction coefficient of the clutch disk, which is an uncertainty in the clutch torque model. Here, the friction coefficient varies depending on various factors such as the temperature of the disk surface, slip speed, and transmission torque. However, since the clutch actuator cannot measure the change in the friction coefficient, it is difficult to calculate an accurate actuator model. As a result of this, a clutch torque that is larger or smaller than expected, such as that shown in (b) of the Fig. 2, is generated by incorrect input. Since clutch 1 and clutch 2 are connected to one final gear due to the structure of DCT, if the torque of the power source is constant, the sum of the clutch torque is constant. Therefore, in the torque phase in which torque is transmitted from the off-going clutch (clutch 1) to the on-coming clutch (clutch 2), if the torque of clutch 2 becomes larger than expected, the torque of clutch 1 rapidly decreases and has a negative value. When tie-up occurs in this way, torque in opposite directions is applied to both ends of the clutch shaft, which may cause damage to the clutch shaft.

However, by using the characteristic of the self-energizing inverse gain of BR-DCT, the magnitude of the negative clutch torque can be reduced when tie-up occurs. Fig. 6 shows the clutch torque when tie-up occurs in the torque phase of BR-DCT. In this figure, it can be seen that the clutch torque decreases faster than the maximum transmitted friction torque of the off-going clutch due to the uncertainty in the coefficient of friction of the on-coming clutch disk. The moment of the torque of the off-going clutch becomes negative, and the maximum transmitted friction torque becomes negative. In the conventional DCT shown by the gray dotted line, the magnitude of the maximum transmitted friction torque in the positive (label A of the Fig.6) and negative directions are the same, so slip occurs only after the negative torque reaches the maximum transmitted friction torque. However, in BR-DCT, since the negative maximum transmitted friction torque (label B of the Fig.6) is determined by G_{inv}, negative maximum transmitted fric-
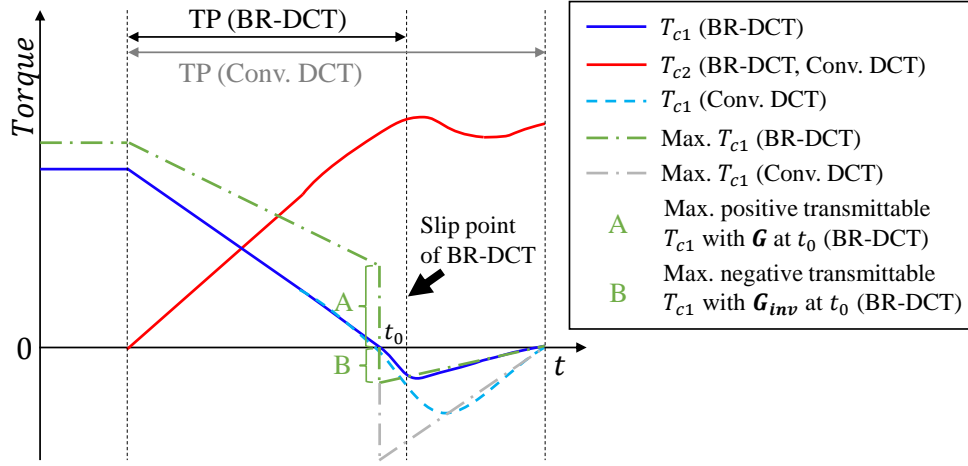
Figure 6: Clutch torque and maximum transmitted friction torque when tie-up occurs in BR-DCT and conventional DCT. Using the fact that the self-energizing gain of BR-DCT varies according to the direction of the clutch torque, it can reduce the tie-up effect.

tion torque becomes smaller than the positive direction. Therefore, clutch slip occurs faster than in conventional DCT (slip point of the Fig. 6), and the maximum value of negative torque decreases. In this way, compared to the conventional DCT, the BR-DCT can reduce the maximum value of the negative direction torque when tie-up occurs. However, to utilize this effect, the design constraint about self-energizing gain is required.

$$G >> G_{inv} \tag{16}$$

In other words, slip occurs faster when the maximum transmitted friction torque in the negative direction is small compared to the positive direction. From (15) and (12), it can be seen that G and G_{inv} have the same numerator and only their denominators are different. Therefore, the change of the denominator is determined according to the change of the design parameter α. In conclusion, it can be seen that the smaller the α, the greater the difference between G and G_{inv}. In general, if α is made smaller, the difference between G and G_{inv} becomes larger. That is, referring to Fig. 3, the slope of the ball-ramp is lowered by reducing the ramp angle, which is closer to the singular point of the self-energizing effect. Therefore, it is important not to excessively decrease the ramp angle.

14

2.2.3. Additional Design Constraints

The parameter design constraints proposed in Section (2.2) of this paper can be summarized as follows.

4. Using (15) as a clutch actuator model and mounting force sensor on the output of the clutch actuator to measure F_a: To calculate the clutch torque.

5. Minimize α : To reduce negative torque when clutch tie-up occurs.

If the BR-DCT design constraints of Section 2.1 and the design constraints proposed in this study are applied together, it is possible to use accurate clutch actuator model and minimize the negative torque when tie-up occurs. As a result of this, the shift control performance of the BR-DCT can be further improved.

Remark 1. *The coefficient of friction is essential in the method of calculating the clutch torque. However, the friction coefficient cannot be measured due to the absence of the torque sensor, and the friction coefficient changes due to various causes such as clutch torque or slip speed. Further, it cannot be estimated without the clutch torque information, and even if it is estimated with the output torque composed of vehicle acceleration, the accuracy thereof is low. In other words, the coefficient of friction is the most necessary value, but it cannot be measured directly. However, BR-DCT can obtain the clutch torque equation expressed in (15) by using the self-energizing principle. Using this equation, it is necessary to measure the clutch actuator force instead of the friction coefficient. However, this method does not completely eliminate the friction coefficient from the clutch torque equation, but it means that the friction coefficient can be replaced by the clutch actuator force. That is, the friction coefficient can be measured indirectly by measuring the clutch actuator force. In fact, using (14), it is possible to measure the friction coefficient indirectly with the force of the actuator. Unlike the method in which the friction coefficient is assumed to be a constant or a table for the actuator position in the DCT shift control, this method means that a measurement close to the actual friction coefficient can be made using the actuator force. That is, since the change in the friction coefficient can be measured, model uncertainty can be greatly reduced compared to the method assuming a constant or a table of the actuator position.*
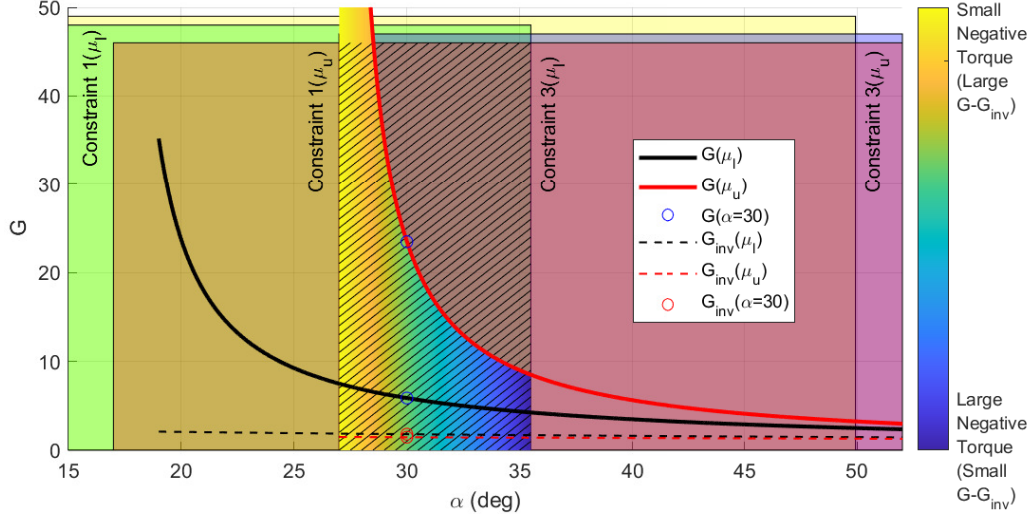
Figure 7: BR-DCT design constraints with G and G_{inv} according to α. The striped area represents the range of α that satisfies all four constraints.

2.3. Selection of Design Parameter

Design parameters were selected using the design constraints of the BR-DCT proposed in the previous study and the additional constraints proposed in this paper. Here, it is assumed that the clutch friction coefficient has a value within a specified range. $(\mu = \{\mu \| \mu_l < \mu < \mu_u\}, \mu_l = 0.3, \mu_u = 0.5)$ Constraints 1, 3, and 5 are all constraints of ramp angle (α). In addition, constraints 1 and 3 can be expressed as the upper and lower bounds of μ, respectively. Therefore, when satisfying the four inequalities for α, it becomes a problem of minimizing α. In Fig. 7, the 4 inequalities were expressed as shaded areas along with changes in G and G_{inv} according to α. Here, to satisfy design constraint 5, the smallest α may be selected in a region where all shades intersect. Referring to design constraint 5, the greater the difference between G and G_{inv}, the smaller the negative torque when tie-up occurs. That is, the tie-up effect can be alleviated. Therefore, this constraint is indicated by a color map under $G(\mu_u)$ in Fig. 7 and a color bar on the right. Considering all constraints, the smallest alpha in the striped area is selected as the optimal point. At this time, parameters were selected in consideration of safety factors and machinability. The selected design parameters are shown in Table 2. Using the selected design parameters, a

16
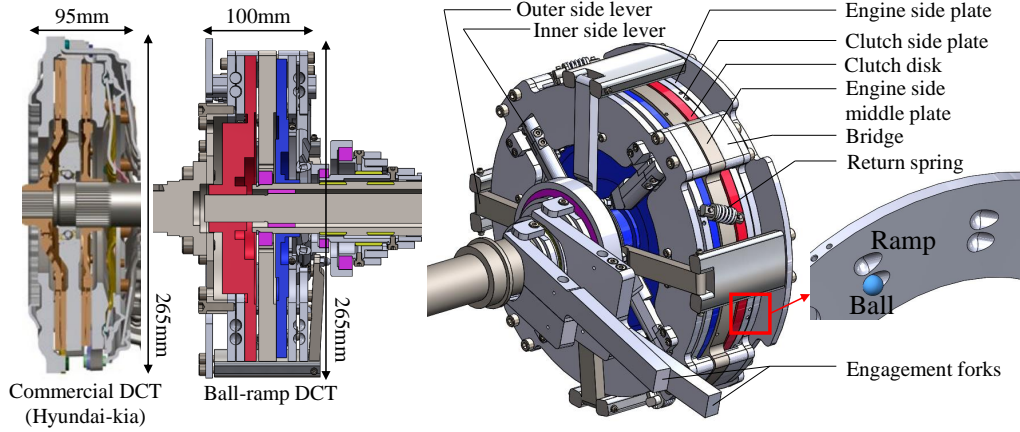
Figure 8: Prototype of the BR-DCT clutch pack. Left: Comparison of cross-section between BR-DCT and commercial DCT clutch pack (Hyundai-Kia [30]). Right: The name of each part of BR-DCT clutch pack and ball-ramp structure.

BR-DCT clutch pack prototype was designed as shown in Fig. 8.

3. Experimental Analysis

3.1. Experimental Setup

To verify the proposed clutch actuator model and tie-up effect reduction of the prototype by applying the proposed BR-DCT design constraints, a test bench that simulates the vehicle's powertrain was designed. All parts

Table 2: Selected design parameters of the BR-DCT

Name	Value
R_a	92.7mm
R_s	119.5mm
R_c	92.7mm
R_b	91mm
α	30°
$\min \beta$	6°
$G(\mu = 0.3)$	8.87
$G_s(\mu = 0.3)$	0.10
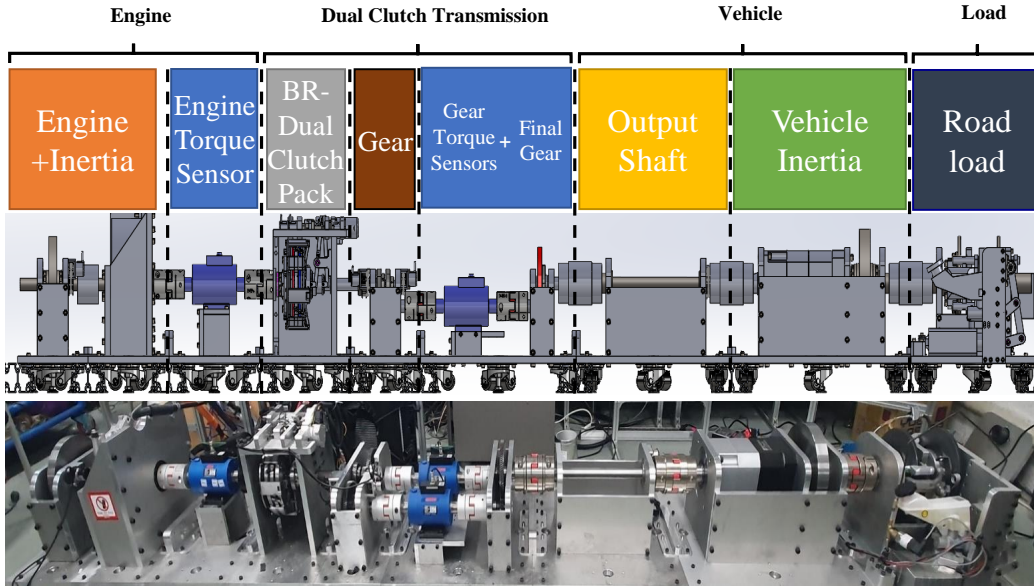
Figure 9: A testbench that simulates the powertrain of a vehicle equipped with BR-DCT. It is equipped with a torque sensor that can measure the torque of the power source and clutch. Each part is designed in module type and can be replaced.

are manufactured in module type and can be exchanged according to the type of experiment.

The test bench consists of a power source, DCT, vehicle, and load module. A Permanent Magnet Synchronous Motor (PMSM) was used as the power source module connected to the rotational inertia, and the BR-DCT module was composed of clutch pack and actuators, gears, torque sensors for verification, and final gear. The force sensor used in the BR-DCT module has a maximum measurable force of 2000N, a resolution of $+1/10,000$, a sampling time of 0.5ms, and guarantees a repeatability error of less than 0.2% R.O. In addition, the optical encoder for measuring the position of the actuator outputs a square wave composed of three phases A, B, and Z, and outputs 300 pulses per rotation of the motor. The specifications of the torque sensor used in this experiment have a maximum measurable torque of 1000Nm, a resolution of $\pm 1/30,000$, a sampling time of 0.5ms, and a repeatability error of less than 0.2% R.O. is guaranteed. In order to reduce the complexity of the system, each shaft on which a torque sensor for verification is installed is fixed to the first and second gears. To verify the tie-up reduction ef-

18

Conv. DCT module   BR-DCT module
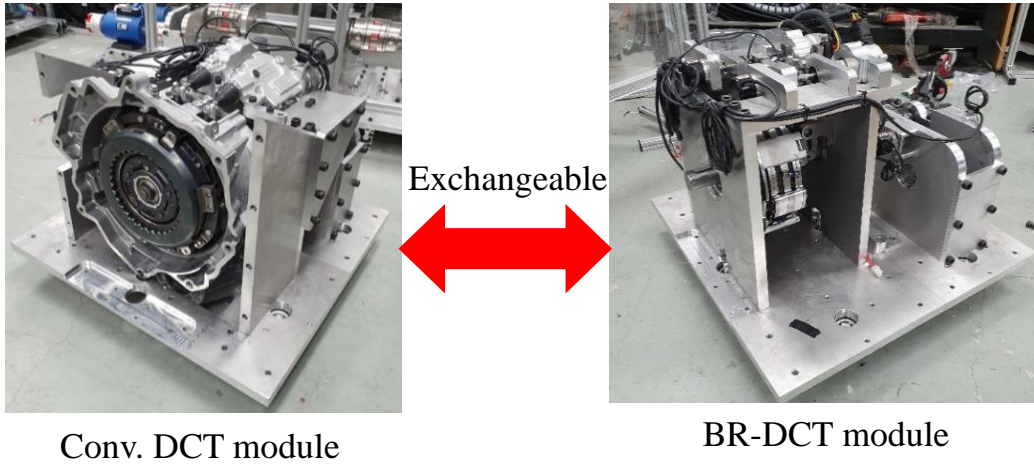
Figure 10: The DCT module of the test bench was designed with conventional DCT and BR-DCT to verify the proposed method.

fect, a conventional DCT module was manufactured using a 6-speed DCT of Hyundai-Kia. (Fig. 10) The conventional DCT module was designed by replacing the clutch pack and actuator from the BR-DCT module.

The vehicle module is composed of a shaft for having compliance for realizing the vibration of the drive shaft, and a disk plate and reduction gear for implementing the body mass. The vehicle module used in the test bench was designed to target 1500kg, which is the weight of a typical passenger car. The load module is designed to generate load torque using an electro-hydraulic brake system.

3.2. Closed Loop Shift Controller

Generally, DCT shifting is characterized by a short torque phase for fast torque exchange and a long inertia phase for smooth acceleration. Since the clutch torques are exchanged in the torque phase, tie-up is easy to occur. Therefore, clutch must be disengaged when the clutch torque becomes zero. Therefore, the shift controller controls to disengage the off-going clutch when the clutch torque becomes zero. At this time, BR-DCT uses an open-loop controller because the clutch is disengaged when a tie-up occurs. In the inertia phase, the on-coming clutch accelerates and the power source decelerates to synchronize the speed. Torque and slip speed reference are planned

19
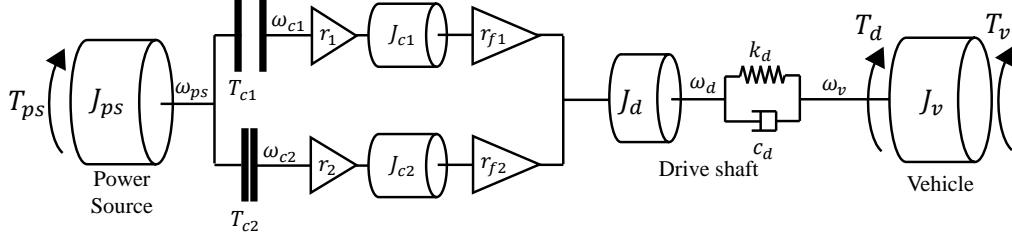
Figure 11: Free body diagram of the vehicle powertrain equipped with BR-DCT.

for smooth and rapid acceleration of the on-coming clutch. At this time, the power source and the on-coming clutch torque are available as inputs. Therefore, the inertia phase controller uses a Multi-Input Multi-Output (MIMO) controller to control the two outputs with two inputs [31, 32].

3.2.1. Target system modeling

The powertrain of a vehicle equipped with BR-DCT can be modeled as shown in Fig. 11.

$$J_{ps}\dot{\omega}_{ps} = T_{ps} - T_{c2} \tag{17}$$

$$J_{c1}\dot{\omega}_{c1} = -\frac{r_2 r_{f2}}{r_1 r_{f1}} T_{c2} - \frac{1}{r_1 r_{f1}} T_d \tag{18}$$

$$J_{c2}\dot{\omega}_{c2} = T_{c2} - \frac{1}{r_2 r_{f2}} T_d \tag{19}$$

$$J_d\dot{\omega}_d = r_2 r_{f2} T_{c2} - T_d \tag{20}$$

$$J_v\dot{\omega}_v = T_d - T_v \tag{21}$$

$$T_d = k_d(\theta_d - \theta_v) + c_d(\omega_d - \omega_v) \tag{22}$$

where, $ps, c1, c2, d$ and v denote power source, clutch 1, clutch 2, drive shaft and vehicle, respectively. In addition, J, T, ω and θ indicate rotational inertia, torque, angle and angular speed of each component. r_1, r_2, r_{f1} and r_{f2} represent the first gear, second gear, first final gear and second final gear ratio, respectively. k_d and c_d represent the stiffness and damping coefficient of the drive shaft. T_v represents road load. In this model, the drive torque transmitted to the vehicle is expressed as the drive shaft torque (T_d).

20

If the inertia of clutches 1 and 2 and the drive shaft are replaced with the equivalent inertia $(J_{c2,eq})$ and the drive shaft speed is expressed as the speed of clutch 2, (17), (18), (19), (20) and (21) are simplified as follows.

$$\dot{\omega}_{ps} - \dot{\omega}_{c2} = \frac{T_{ps}}{J_{ps}} - \left(\frac{1}{J_{ps}} + \frac{(r_2 r_{f2})^2}{J_{c2,eq}}\right)T_{c2} + \frac{r_2 r_{f2}}{J_{c2,eq}}T_d \tag{23}$$

$$\frac{\dot{\omega}_{c2}}{r_2 r_{f2}} - \dot{\omega}_v = -\left(\frac{1}{J_{c2,eq}} + \frac{1}{J_v}\right)T_d + \frac{r_2 r_{f2}}{J_{c2,eq}}T_{c2} + \frac{1}{J_v}T_v \tag{24}$$

$$\dot{T}_d = k_d\left(\frac{\omega_{c2}}{r_2 r_{f2}} - \omega_v\right) - c_d\left(\frac{1}{J_{c2,eq}} + \frac{1}{J_v}\right)T_d + \frac{c_d r_2 r_{f2}}{J_{c2,eq}}T_{c2} + \frac{c_d}{J_v}T_v \tag{25}$$

$$where, J_{c2,eq} = (r_2 r_{f2})^2 J_{c2} + (r_1 r_{f1})^2 J_{c1} + J_d \tag{26}$$

Reduced powertrain dynamics is expressed in state space using slip speed $(\omega_{ps} - \omega_{c2} = \omega_{slip})$, drive shaft compliance rate $(\omega_d - \omega_v)$ and drive torque (T_d) as state, and slip speed and drive torque as output.

$$\dot{\mathbf{x}} = \mathbf{A}\mathbf{x} + \mathbf{B}\mathbf{u} + \mathbf{E}\boldsymbol{\delta}$$

$$where, \mathbf{x} = \begin{bmatrix} \omega_{ps} - \omega_{c2} \\ \frac{\omega_{c2}}{r_2 r_{f2}} - \omega_v \\ T_d \end{bmatrix}, \mathbf{u} = \begin{bmatrix} T_{ps} \\ T_{c2} \end{bmatrix}, \boldsymbol{\delta} = T_v,$$

$$\mathbf{A} = \begin{bmatrix} 0 & 0 & \frac{r_2 r_{f2}}{J_{c2,eq}} \\ 0 & 0 & -\left(\frac{1}{J_{c2,eq}} + \frac{1}{J_v}\right) \\ 0 & k_d & -c_d\left(\frac{1}{J_{c2,eq}} + \frac{1}{J_v}\right) \end{bmatrix}, \mathbf{E} = \begin{bmatrix} 0 \\ \frac{1}{J_v} \\ \frac{c_d}{J_v} \end{bmatrix},$$

$$\mathbf{B} = \begin{bmatrix} \frac{1}{J_{ps}} & -\left(\frac{1}{J_{ps}} + \frac{(r_2 r_{f2})^2}{J_{c2,eq}}\right) \\ 0 & \frac{r_2 r_{f2}}{J_{c2,eq}} \\ 0 & \frac{c_d r_2 r_{f2}}{J_{c2,eq}} \end{bmatrix} \tag{27}$$

3.2.2. Multi-variable Controller Design

The target system has various system uncertainties such as nonlinearity of clutch disk friction coefficient, load torque (T_v), and gear backlash. To be robust against this uncertainty, a robust shift controller such as $\mathcal{H}_\infty$ controller is used [31, 33]. Therefore, in this paper, an $\mathcal{H}_\infty$ loop shaping controller that is robust against uncertainty and can adjust the frequency response was selected.
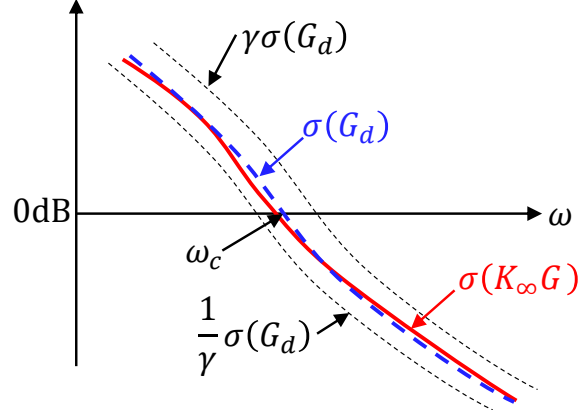
Figure 12: Conceptual diagram of a $\mathcal{H}_\infty$ loop shaping controller $(K_\infty(s))$ that satisfies $G_s(s) \to G_d(s)$ as much as possible and maximizes uncertainty bound.

The objective of $\mathcal{H}_\infty$ loop shaping controller is to design pre-compensator $W(s)$ that satisfies:

$$G_s(s) = W(s)G(s) \to G_d(s) \tag{28}$$

and controller $K_\infty(s)$ that maximizes uncertainty bound γ:

$$K_\infty(s)G_s(s) = K(s)W(s)G(s) \tag{29}$$

where, $G_d(s)$ is a desired plant, $G_s(s)$ is a shaped plant, $K_\infty(s)$ is $\mathcal{H}_\infty$ loop shaping controller.

The $\mathcal{H}_\infty$ loop shaping controller $K_\infty(s)$ satisfies $G_s(s) \to G_d(s)$ as much as possible and aims to maximize the uncertainty bound γ. This purpose can be expressed graphically as in the Fig. 12. Also, it can be expressed as the following equation.

$$\underline{\sigma}(G_sK_\infty) \geq \frac{1}{\gamma}\underline{\sigma}(G_d), \bar{\sigma}(G_sK_\infty) \leq \gamma\bar{\sigma}(G_d) \tag{30}$$

Here, $\underline{\sigma}(\cdot)$ represents the minimum singular value, $\bar{\sigma}(\cdot)$ represents the maximum singular value, and γ represents the boundary where $K_\infty(s)G_s(s)$ exists based on $G_d(s)$. That is, it represents the range in which a controlled plant can exist according to the maximum value of uncertainty. Since the size of this boundary is determined according to the shape of $G_d(s)$, using (30), $K_\infty(s)$ can be obtained using the following equation.

22
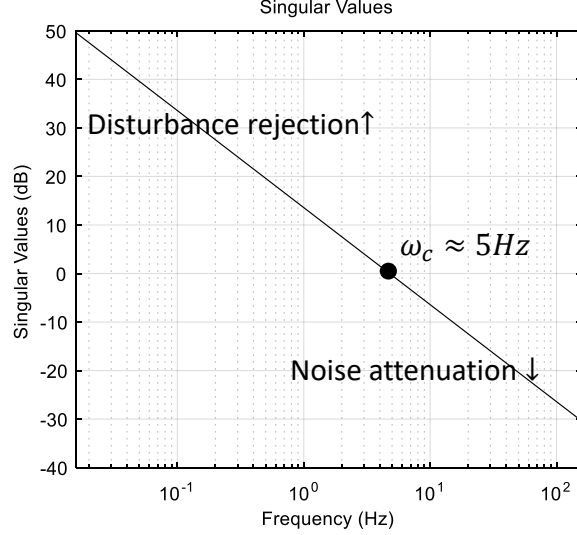
Figure 13: Frequency response of desired plant (G_d)

$$\gamma = \min_{K_\infty} \left\| \begin{bmatrix} I \\ K_\infty \end{bmatrix} (I - G_s K_\infty)^{-1} \begin{bmatrix} G_s & I \end{bmatrix} \right\|_{\mathcal{H}_\infty} \tag{31}$$

To find optimal value of the $\mathcal{H}_\infty$ loop shaping controller $K_\infty(s)$ satisfies $G_s(s) \to G_d(s)$ as much as possible and aims to maximize the uncertainty bound γ, Riccati equations are used[34].

Here, the $G_d(s)$ is designed to have a 5Hz cutoff frequency (ω_c) to improve low-frequency disturbance rejection performance and reduce high-frequency noise attenuation. (Fig. 13) The H_∞ loop shaping controller is designed using a method that minimizes a function that takes robustness against model uncertainty as a cost [35].

As can be seen from the singular value plot (Fig. 14) of the $G(s)$ with stabilizing controller $K(s)$'s open-loop and closed-loop transfer function, a shaped plant that matches the desired plant can be obtained.

Since the purpose of this paper is to improve the actuator uncertainty and tie-up of BR-DCT only as a design constraint, the control strategy generally used methods found in the literature. However, since the improvement of performance may be limited only by improving the hardware, improvement

23
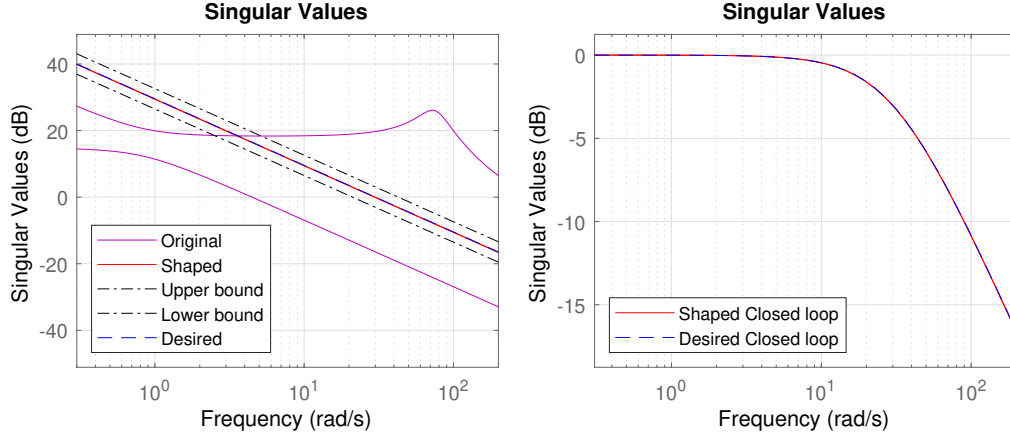
Figure 14: Frequency response of original, desired, shaped and closed loop transfer functions.

of shift performance using a control strategy is being studied as a future work.

3.3. Validation of reduction of the uncertainties in the actuator model

3.3.1. Launch (forward) experiment for G

To verify the reduction of the uncertainties in the clutch actuator proposed in Section 2.2.1, an experiment was performed to measure G when the vehicle launches. From the relationship between $T_c = \mu R_c N$ and (15), the self-energizing gain (G) can be measured. Using this relationship, (8) can be written as follows.

$$N(\theta_{BR}) = G(\theta_{BR}, \mu)F_a - G_s(\theta_{BR}, \mu)F_s(\theta_{BR}) \tag{32}$$

Here, the mapping of the F_s according to θ_{BR} is determined at the design stage, it can be measured using actuator position (θ_{BR}). N can be calculated through compression modeling of the clutch disk. That is, it can be expressed as $N = K\Delta$ and Δ can be measured through the encoder (θ_{BR}) of the clutch actuator. Also, μ can be measured with a clutch torque sensor and N for verification. (using $T_c = \mu R_c N$) Summarizing this, the self-energizing gain (G) can be measured with the following equation:

$$G = \frac{R_b \tan \alpha + LR_a}{R_b \tan \alpha - \mu R_c} = \frac{N(\theta_{BR}) + G_s(\theta_{BR}, \mu)F_s(\theta_{BR})}{F_a} \tag{33}$$

24
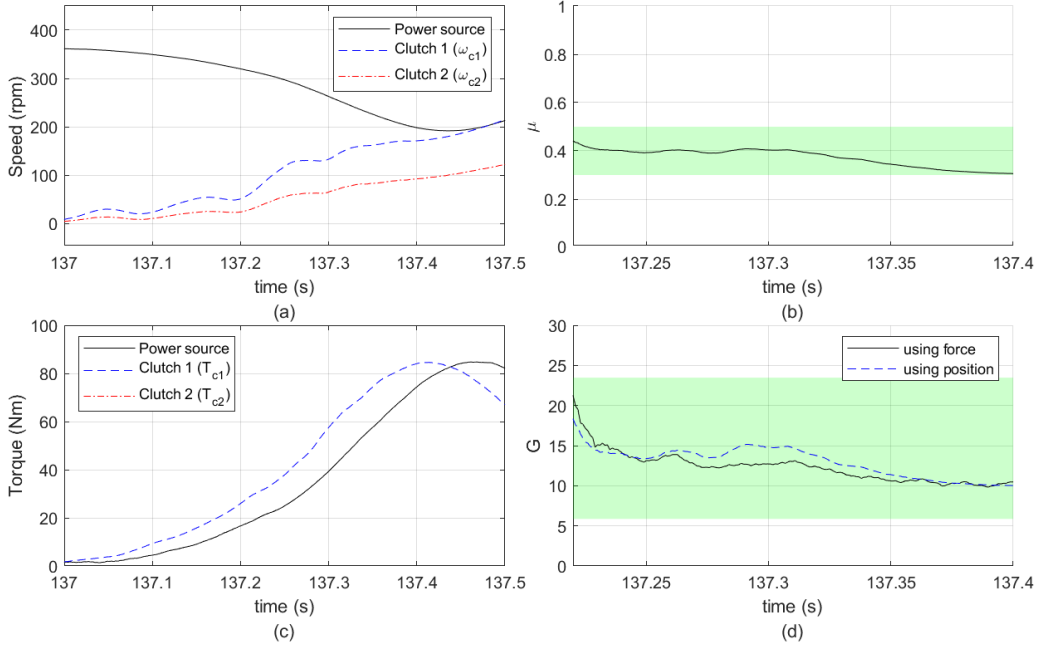
Figure 15: Launch experiment result for verifying self-energizing gain(G) of BR-DCT.

The launch experiment scenario is as follows. First, when the power source maintains the speed using the speed controller, a ramp input is applied to the actuator of clutch 1 to generate clutch torque. Due to the generation of clutch torque, the speed of the power source decreases. The speed controller generates a power source torque to maintain the speed. At this time, clutch torque is generated in proportion to the force applied by the actuator. Therefore, as the actuator force is generated and the clutch torque increases, the speed of the power source decreases. As a result, the power source torque increases more slowly than the clutch torque. As a result of the Launch experiment, the clutch friction coefficient can be measured by using the torque sensor for verification and (14). In general, the dry DCT's clutch friction coefficient is in the range of $0.3 - 0.5$. In addition, the self-energizing gain can be measured using equation (33). When considering the change in friction coefficient, the self-energizing gain (G) and self-energizing inverse gain (G_{inv}) to be verified in this scenario are expected to be $5.87 - 23.47$ and $1.47 - 1.81$, respectively. These results are shown in Fig. 15.

Referring to (a) of Fig. 15, the power source maintains 370 rpm, and then

the speed decreases due to the increase of clutch torque from 137 seconds. Here, the friction coefficient of the clutch disk can be obtained using (14) ((b) of the Fig. 15), but the exact friction coefficient cannot be measured because the clutch is in contact without compression when the contact of the clutch disk starts (137.1 seconds). Therefore, the friction coefficient was measured from the start of clutch compression. The self-energizing gain (G) was also measured from the start of clutch compression. ((d) of the Fig. 15) As mentioned earlier, the friction coefficient was measured in the range of $0.3 - 0.5$. Accordingly, it can be seen that the self-energizing gain (G) is measured within the expected range of $5.87 - 23.47$. Also, it can be seen that the value measured using force and position measurement with the right side of (33) is almost accurate to the value measured using position and μ measurement with the left side of (33). However, an error occurred between the measured values. This can be seen as uncertainty in the model due to the measurement error of the actuator force sensor. As shown in Fig. 5, the force sensor is attached to the actuator output, not in the clutch pressure plate. Measuring forces at this location yields measurements including uncertainties due to friction or deformation of the parts. This uncertainty leads to errors in self-energizing gain (G) measurements and clutch actuator models. Therefore, how to estimate these uncertainties will be discussed in future work.

3.3.2. Launch (backward) experiment for G_{inv}

Fig. 16 shows the experimental results for verification of self-energizing inverse gain (G_{inv}) in the same scenario as the above experiment. In this experiment, when the power is controlled at $-400rpm$ with an individual controller, the target position of the clutch 1 actuator is increased to increase the clutch torque. As a result of this experiment, the friction coefficient was measured in the range of $0.3 - 0.5$. Also, the measurement result of self-energizing inverse gain (G_{inv}) was inside the expected range $(1.47 - 1.81)$. However, the difference between measured values using force and position measurement and position and μ measurement is greater than the self-energizing gain verification. The cause of this difference can be seen as a measurement error in the force sensor due to friction between parts as in the self-energizing gain verification experiment. Therefore, in order to accurately measure the self-energizing inverse gain, it is necessary to estimate the uncertainty of the clutch actuator. And it can be confirmed that the self-energizing inverse gain (G_{inv}) measured through this experiment always has a smaller value than the self-energizing gain (G). (Fig. 17) Summarizing
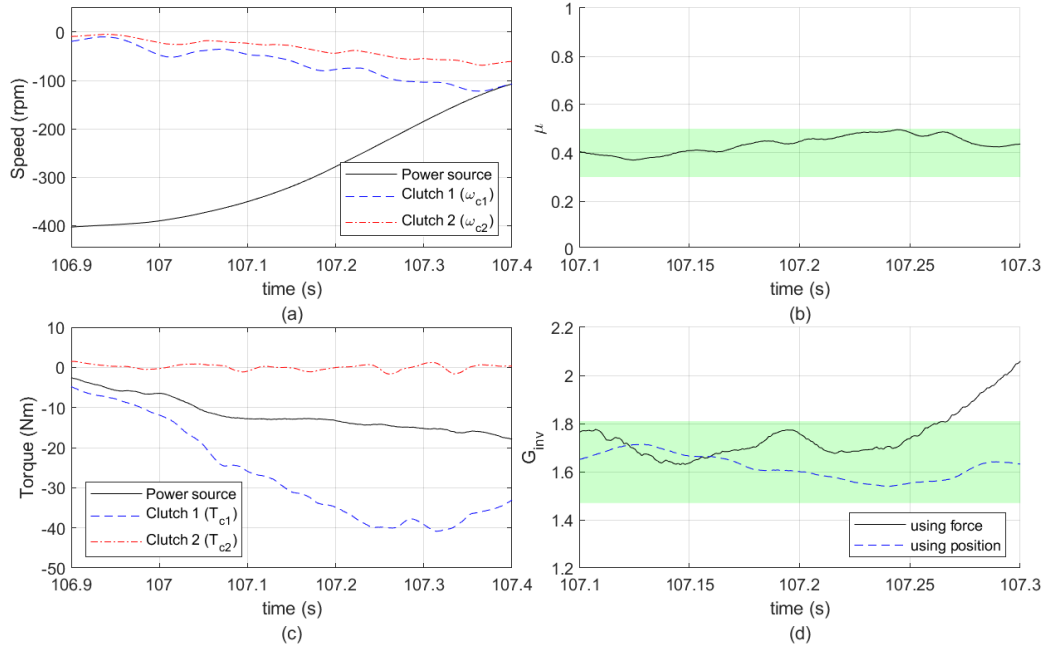
Figure 16: Reverse launch experiment result for verifying self-energizing inverse gain(G_{inv}) of BR-DCT.
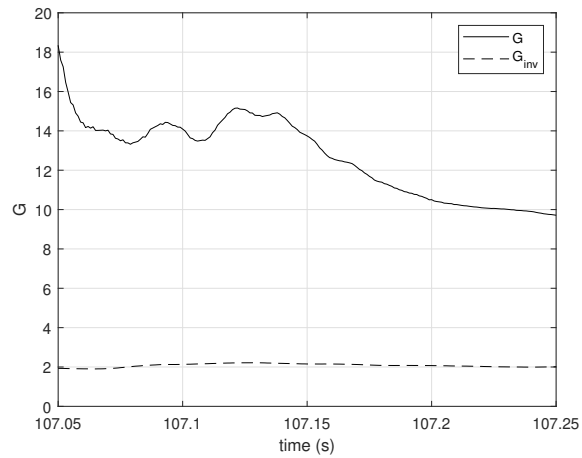
Figure 17: Comparison of the magnitude of G and G_{inv} measured through launch experiments.

these results, the tie-up effect during TP control is alleviated by designing the self-energizing gain (G) to be larger than the self-energizing inverse gain (G_{inv}).

3.3.3. Up-shift experiment for model validation

As mentioned earlier, one of the biggest advantages of the BR-DCT is that the friction coefficient can be removed from the clutch actuator model. That is, the clutch torque can be configured using only the position of the clutch actuator and the force sensor. In this case, the model of the clutch actuator can use (15). For verification, an experimental scenario was selected based on the phases that require an accurate actuator model among shift scenarios. The shift experiment scenario is composed as follows. First, when clutch 1 is engaged with the power source, a constant torque is generated from the power source and the vehicle accelerates. When the shift target speed is reached, a torque phase begins in which torque is transmitted to the on coming clutch. When the torque of the off-going clutch becomes zero, the inertia phase is initiated, which synchronizes the speed of the power source and the on coming clutch. In this case, the H_∞ shift controller (Section 3.2) is used to track the references. In this scenario, using the inverse model of the improved clutch actuator model of equation (15), the clutch torque can be calculated from the actuator's position and force. For comparison, torque calculation results using the actuator inverse model of the conventional DCT in which clutch torque is expressed as constant μ and normal force were used. The equation used in this model is as follows.

$$T_c = \mu R_c N(\theta_m) = \mu f(\theta_m) \tag{34}$$

The μ of the conventional DCT is generally assumed to be a predefined table about actuator position because it is unknown with in-vehicle sensors. Therefore, when the clutch slips and the change in the actuator position is reduced, the change in the value of the friction coefficient is also reduced. As a result, the friction coefficient actually changes, but the conventional DCT uses a nearly constant value of μ. Thus, a large model error occurs due to changes of μ due to slip speed or disk surface temperature. In (34), N can be expressed as a function of θ_m. Here, θ_m is the position of the actuator measured by the encoder. That is, the clutch torque model of the conventional DCT uses only the actuator position measurement value.

In Fig. 18, the power source is controlled with a torque of $21Nm$ while being engaged with clutch 1. Referring the (a) of the Fig. 18, when the

28
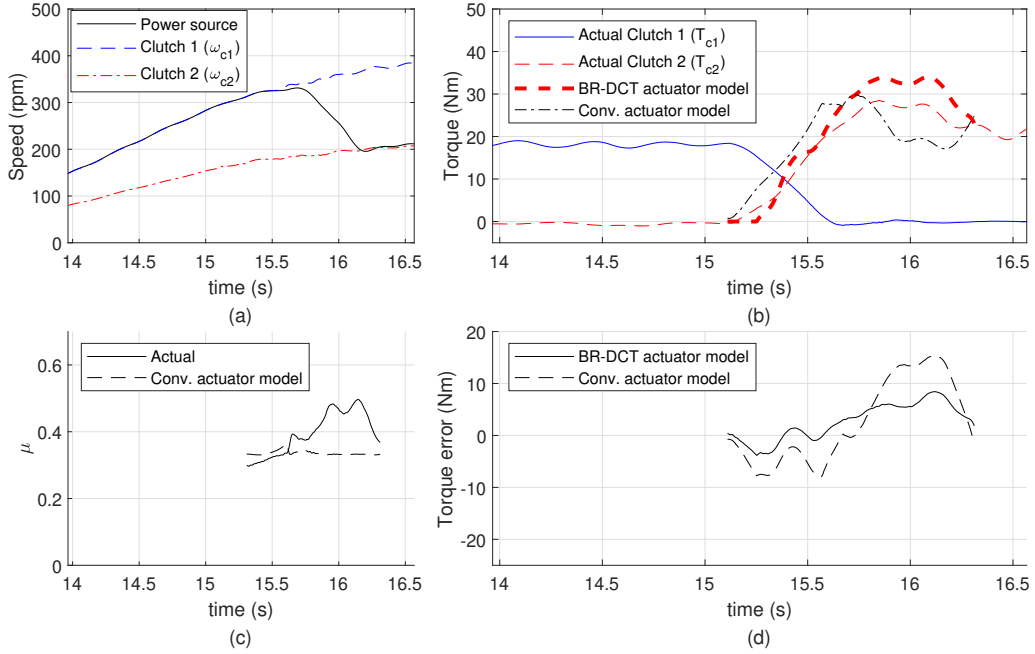
Figure 18: Up-shift experiment result to compare the improved actuator model accuracy of BR-DCT by using the proposed design constraints with conventional DCT.

Table 3: Comparison of the actuator model accuracy

Index	Conv. DCT	BR-DCT
RMS error	$8.40Nm$	$4.36Nm$
Maximum error	$15.36Nm$	$8.42Nm$

speed of clutch 1 reaches 300 rpm (15.1 seconds), the torque phase starts and a shift command is applied to the controller. Referring to (b) of Fig. 18, the torque calculation using the inverse model of the clutch actuator started with the start of the shift, and the difference between the value measured by the torque sensor and the value calculated by the inverse model is shown in (d) of Fig. 18 and Table 3. The maximum error of the torque calculated using the inverse actuator model of BR-DCT was measured to be within $9Nm$, while the maximum error of the torque calculated using the inverse actuator model of the conventional DCT was measured to be $15Nm$. Referring to the (c) of Fig. 18, as the error between the actual μ and the μ used in the model of conventional DCT increases, the torque error increases. Referring to Table 3, the RMS value of the error of the torque calculation value using BR-DCT is 48% smaller. That is, the clutch torque calculation value using the inverse actuator model of BR-DCT has high accuracy even without measuring μ. However, the torque calculation value using the inverse actuator model of BR-DCT still has an error of $9Nm$. Specifically, the error is small in the torque phase, whereas the error increases in the inertia phase. When referring to the calculation error of clutch 2, the error also increases as the clutch torque increases. As mentioned above, this error may be caused by an error of the sensor for the measurement of F_a, a change in the lever model, and a change in parameters of the powertrain model. However, the parameters of the powertrain model have already been verified for accuracy through verification work, and the change of the lever model was measured to be negligible. In addition, the error increases as the actuator force increases. Since the friction force between the parts increases as the actuator force increases, it can be seen that the measurement error of F_a due to friction between the actuator parts is dominant in the clutch torque measurement error. This error has a much smaller value than the actuator model uncertainty of the conventional DCT, but still needs to be estimated. Therefore, a follow-up study to estimate the disturbance composed of friction between parts is in progress.

3.4. Validation of Reduction of Tie-up Effect

To verify the design constraints so as to reduce the magnitude of negative torque in the tie-up proposed in Section 2.2.2, a shift experiment was conducted to measure the torque of the clutch when the vehicle shifts. This experiment selected the same shifting scenario as in Section 3.3.3. However, to induce the tie-up phenomenon, torque phase control was performed by
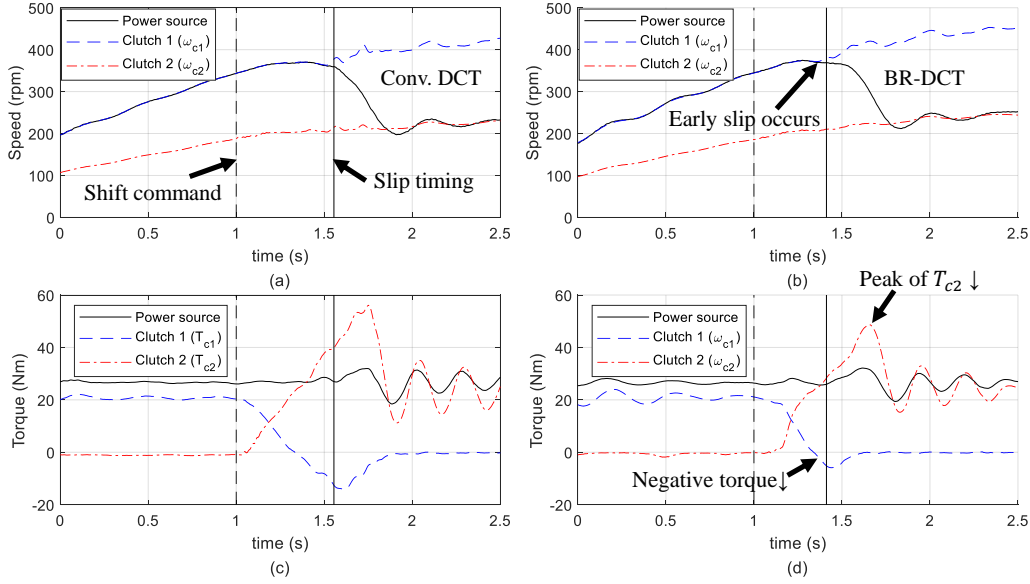
Figure 19: Up-shift experiment results to compare the magnitude of negative torque with conventional DCT when tie-up occurs in BR-DCT with proposed design constraint applied.

adding a friction coefficient uncertainty to the clutch actuator model. Inertia phase control was not performed to measure the increase in shift shock due to negative torque when tie-up occurs. To verify the reduction of the tie-up effect of BR-DCT, conventional DCT and BR-DCT were tested in the same scenario. To verify the design method proposed in this paper, this experiment assumes that the disturbance compensation control is impossible due to unexpected actuator uncertainty. In other words, before mitigating the tie-up effect using the control method, we want to evaluate whether the tie-up effect can be mitigated with hardware design alone.

Fig. 19 shows the experimental results for a scenario inducing the occurrence of tie-up in conventional DCT and BR-DCT. Referring to (a) and (b) of Fig. 19, the shift command is applied from 1 second, and both DCTs perform torque phase control. Referring to (c) and (d) of Fig. 19, due to the artificially added clutch friction coefficient uncertainty, the torque of clutch 2 increases rapidly, and the torque of clutch 1 decreases, resulting in a negative value. In conventional DCT, after tie-up occurred, the negative torque of clutch 1 increased to $17Nm$ and the torque phase lasted about 0.6 seconds. However, in BR-DCT, the negative torque increased only up to $6Nm$,
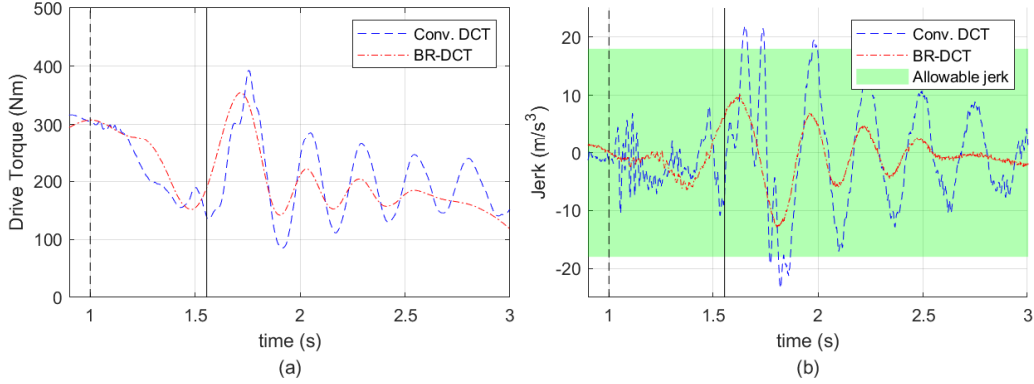
Figure 20: The drive torque and jerk to evaluate tie-up reduction effects.

Table 4: Comparison of the reduction of tie-up effect

Index	Conv. DCT	BR-DCT
Maximum jerk	$21.98m/s^3$	$11.24m/s^3$
25% settling time	$1.24s$	$0.47s$

and the torque phase was terminated relatively quickly after the negative torque was generated and lasted for about 0.45 seconds. In other words, BR-DCT minimizes the negative torque of clutch 1 because slip occurs faster than in conventional DCT. These results were obtained using only differences in hardware, without changing the controller. In addition, it is possible to know where the reduction in the tie-up effect is improved through additional evaluation indexes.

In Fig. 20, drive torque and jerk are plotted as the result of Fig. 19. Referring to (b) of Fig. 20, the jerk of Conventional DCT has risen to a maximum of $21.98m/s^3$, but in the BR-DCT, the jerk is up to $11.24m/s^3$, which is about 49% lower. The maximum allowable jerk in a typical passenger car is known to be $18m/s^3$ [36]. Referring to (b) of Fig. 20, the shift shock caused by the tie-up of the conventional DCT exceeds the allowable jerk, but the BR-DCT is only about 62% of the maximum value. This means that the shift shock felt by the driver is reduced by 49%. Referring to (a) of Fig. 20, it can be seen that the settling time of BR-DCT vibration is also shortened by 62%. That is, the duration of the vibration felt by the driver may be shortened. These indexes are organized in Table. 4 As a result, the

improvement of the shift control performance was verified through experiments when the design constraints for reducing the magnitude of negative torque in the tie-up proposed in Section 2.2.2 are satisfied. This tie-up mitigation effect is an advantage of BR-DCT along with the improved actuator model that reduces the uncertainty verified in Section 3.3.3.

4. Conclusion and Future Work

BR-DCT could have several advantages compared to conventional DCT. In particular, if the self-energizing principle is used, the model uncertainty can be reduced because the clutch actuator model with the friction coefficient removed can be used. In addition, it is possible to minimize the vibration felt by the driver when a tie-up occurs. However, in the previous study dealing with the design method of BR-DCT, only design constraints to reduce energy consumption were considered. In this paper, based on the existing design method of BR-DCT, design constraints for reducing the uncertainties in the actuator model and reducing vibration in tie-up are added. Therefore, the contribution of this paper is to improve the shift control performance by optimizing the existing model of BR-DCT. A powertrain test bench was used to verify the proposed design constraints. In this case, unlike previous studies, the verification method was improved by performing a shift experiment using a closed-loop shift controller. Since the experimental scenario consisted of launch and shift, it was possible to perform verification in various situations. As a result of the verification experiment, the clutch torque calculation error using only the measured value of the clutch actuator without the friction coefficient was reduced by 48% compared to the existing method. In addition, when the tie-up phenomenon occurred, the magnitude of vibration due to tie-up was reduced by 49% in BR-DCT compared to conventional DCT, and the duration was reduced by 62%. As a result, the shift shock felt by the driver can be reduced. If the BR-DCT is designed using the two design constraints proposed in this paper, it can be expected that the shift control performance will be improved compared to the conventional DCT.

However, it is difficult to use improved actuator model accurately due to the mounting issue of the force sensor. Specifically, a force sensor should be installed to measure the force (F_a) inside the clutch pack. However, because it is difficult to mount the sensor inside the clutch pack, it was installed at the output of the clutch actuator. In other words, the friction of the parts between the force and the sensor and changes in the actuator model distort

the measured value of F_a. For this reason, the calculated value of clutch torque using BR-DCT shows a difference of about 4Nm compared to the actual value. Therefore, a disturbance observer is needed to estimate the uncertainty of the clutch actuator. However, the BR-DCT clutch actuator model has nonlinearity, so a nonlinear disturbance observer must be used. In addition, there is a possibility of tie-up due to wear of the clutch or aging of the return spring. This problem can be solved by modifying the touch point using slow varying parameter identification. This method will be discussed in a follow-up study on the transmission controller of BR-DCT to which the design method proposed in this paper is applied. Follow-up research on this content is currently in progress.

5. Acknowledgments

References

[1] A. Irimescu, L. Mihon, G. Pãdure, Automotive transmission efficiency measurement using a chassis dynamometer, International Journal of Automotive Technology 12 (4) (2011) 555–559.

[2] A. Turner, K. Ramsay, R. Clark, D. Howe, Direct-drive rotary-linear electromechanical actuation system for control of gearshifts in automated transmissions, in: 2007 IEEE Vehicle Power and Propulsion Conference, IEEE, 2007, pp. 267–272.

[3] H. Kuroiwa, N. Ozaki, T. Okada, M. Yamasaki, Next-generation fuel-efficient automated manual transmission, Hitachi Review 53 (4) (2004) 205–209.

[4] J. Franco, M. A. Franchek, K. Grigoriadis, Real-time brake torque estimation for internal combustion engines, Mechanical Systems and Signal Processing 22 (2) (2008) 338–361.

34

[5] G. Lucente, M. Montanari, C. Rossi, Modelling of an automated manual transmission system, Mechatronics 17 (2-3) (2007) 73–91.

[6] M. Kulkarni, T. Shim, Y. Zhang, Shift dynamics and control of dual-clutch transmissions, Mechanism and machine theory 42 (2) (2007) 168–182.

[7] E. Galvagno, M. Velardocchia, A. Vigliani, Dynamic and kinematic model of a dual clutch transmission, Mechanism and machine theory 46 (6) (2011) 794–805.

[8] S. I.-N. Delhi, Automatic transmissions—amt takes on at, cvt, dct, Auto Tech Review 12 (5) (2016) 20–23.

[9] C. H. F. Amendola, M. A. L. Alves, Gear shift strategies analysis of the automatic transmission in comparison with the double clutch transmission, Tech. rep., SAE Technical Paper (2006).

[10] B. Matthes, Dual clutch transmissions–lessons learned and future potential, SAE transactions (2005) 941–952.

[11] U. Wagner, R. Berger, M. Ehrlich, M. Homm, Electromotoric actuators for double clutch transmissions, in: 8th LuK symposium, 2006.

[12] C.-Y. Cho, J.-H. Kam, H.-K. Hong, C. Lövenich, More efficiency with the dry seven-speed dual-clutch transmission by hyundai, ATZ worldwide 118 (6) (2016) 38–41.

[13] W. Grosspietsch, J. Sudau, Dual clutch for powershift transmissions-a traditional engaging element with new future?, VDI BERICHTE 1565 (2000) 259–274.

[14] D.-H. Kim, J.-W. Kim, S. B. Choi, Design and modeling of energy efficient dual clutch transmission with ball-ramp self-energizing mechanism, IEEE Transactions on Vehicular Technology 69 (3) (2019) 2525–2536.

[15] J. Park, S. Choi, J. Oh, J. Eo, Adaptive torque tracking control during slip engagement of a dry clutch in vehicle powertrain, Mechanism and Machine Theory 134 (2019) 249–266.

[16] S. Kim, S. Choi, Control-oriented modeling and torque estimations for vehicle driveline with dual-clutch transmission, Mechanism and Machine Theory 121 (2018) 633–649.

[17] S. Kim, J. J. Oh, S. B. Choi, Driveline torque estimations for a ground vehicle with dual-clutch transmission, IEEE Transactions on Vehicular Technology 67 (3) (2017) 1977–1989.

[18] J. J. Oh, J. S. Eo, S. B. Choi, Torque observer-based control of self-energizing clutch actuator for dual clutch transmission, IEEE Transactions on Control Systems Technology 25 (5) (2016) 1856–1864.

[19] U. Wagner, A. Wagner, Electrical shift gearbox (esg)-consistent development of the dual clutch transmission to a mild hybrid system, Tech. rep., SAE Technical Paper (2005).

[20] I. Evtimov, R. Ivanov, M. Sapundjiev, Energy consumption of auxiliary systems of electric cars, in: MATEC Web of Conferences, Vol. 133, EDP Sciences, 2017, p. 06002.

[21] G. Leen, D. Heffernan, Expanding automotive electronic systems, Computer 35 (1) (2002) 88–93.

[22] H. Chen, B. Gao, Nonlinear estimation and control of automotive drivetrains, Springer Science & Business Media, 2013.

[23] J. Kim, S. B. Choi, Design and modeling of a clutch actuator system with self-energizing mechanism, IEEE/ASME Transactions on Mechatronics 16 (5) (2010) 953–966.

[24] J. Kim, S. B. Choi, Self-energizing clutch actuator system: Basic concept and design, in: Proceedings of FISITA 2010 World Automotive Congress, 2010.

[25] J. J. Oh, J. Kim, S. B. Choi, Design of self-energizing clutch actuator for dual-clutch transmission, IEEE/ASME Transactions on Mechatronics 21 (2) (2015) 795–805.

[26] J. J. Oh, S. B. Choi, Real-time estimation of transmitted torque on each clutch for ground vehicles with dual clutch transmission, IEEE/ASME Transactions on Mechatronics 20 (1) (2014) 24–36.

[27] J. J. Oh, J. S. Eo, S. B. Choi, Torque observer-based control of self-energizing clutch actuator for dual clutch transmission, IEEE Transactions on Control Systems Technology 25 (5) (2016) 1856–1864.

[28] J. Kim, J. Oh, S. B. Choi, Nonlinear estimation method of a self-energizing clutch actuator load, in: 2012 First International Conference on Innovative Engineering Systems, IEEE, 2012, pp. 231–236.

[29] S. Wang, Y. Liu, Z. Wang, P. Dong, Y. Cheng, X. Xu, P. Tenberge, Adaptive fuzzy iterative control strategy for the wet-clutch filling of automatic transmission, Mechanical Systems and Signal Processing 130 (2019) 164–182.

[30] C.-Y. Cho, J.-H. Kam, H.-K. Hong, C. Lövenich, More efficiency with the dry seven-speed dual-clutch transmission by hyundai, ATZ worldwide 118 (6) (2016) 38–41.

[31] S. Kim, S. B. Choi, Cooperative control of drive motor and clutch for gear shift of hybrid electric vehicles with dual-clutch transmission, IEEE/ASME Transactions on Mechatronics 25 (3) (2020) 1578–1588.

[32] D.-H. Kim, S. B. Choi, Clutch torque estimation of ball-ramp dual clutch transmission using higher order disturbance observer, in: 2020 20th International Conference on Control, Automation and Systems (ICCAS), IEEE, 2020, pp. 743–749.

[33] Z.-G. Zhao, H.-J. Chen, Y.-Y. Yang, L. He, Torque coordinating robust control of shifting process for dry dual clutch transmission equipped in a hybrid car, Vehicle System Dynamics 53 (9) (2015) 1269–1295.

[34] K. Glover, D. McFarlane, Robust stabilization of normalized coprime factor plant descriptions with h/sub infinity/-bounded uncertainty, IEEE transactions on automatic control 34 (8) (1989) 821–830.

[35] D.-H. Kim, S. Choi, Slip speed and drive torque planning of multivariable controller for an electrified vehicle with dual clutch transmission, Tech. rep., SAE Technical Paper (2020).

[36] T. D. Gillespie, Fundamentals of vehicle dynamics, Tech. rep., SAE Technical Paper (1992).